

General COHERENT Constraints on Neutrino Non-Standard Interactions

C. Giunti*

Istituto Nazionale di Fisica Nucleare (INFN), Sezione di Torino, Via P. Giuria 1, I-10125 Torino, Italy

(Dated: 1 September 2019)

We present the results of a systematic study of the constraints on neutrino neutral-current non-standard interactions (NSI) that can be obtained from the analysis of the COHERENT spectral and temporal data. First, we consider for the first time the general case in which all the ten relevant neutral-current NSI parameters are considered as free. We show that they are very weakly constrained by the COHERENT data because of possible cancellations between the up and down quark contributions. However, the up-down average parameters are relatively well constrained and the strongest constraints are obtained for an optimal up-down linear combination of NSI parameters. We also consider the case in which there are only NSI with either up or down quarks, and we show that the LMA-Dark fit of solar neutrino data is excluded at 5.6σ and 7.2σ respectively, for NSI with up and down quark. We finally present the tight constraints that can be obtained on each NSI parameter if it is the dominant one, assuming that the effects of the others are negligible.

I. INTRODUCTION

Coherent elastic neutrino-nucleus scattering (CE ν NS) has been observed recently for the first time in the COHERENT experiment [1], many years after its prediction [2–4]. Several analyses of the COHERENT data provided interesting information on nuclear physics [5–10], neutrino properties and interactions [8–17], and weak interactions [7–10, 18]. In particular, several authors constrained the parameters of neutrino non-standard interactions (NSI) [8, 9, 11–14]. However, in those studies the constraints have been derived by considering only one or two of the NSI parameters as non-vanishing or by considering only NSI interactions with either up or down quarks [11]. In this paper we present for the first time the general COHERENT constraints on the relevant NSI parameters obtained with a fit of the COHERENT data in which all the NSI parameters are considered as free.

Our calculations implement the improved quenching factor in Ref. [19] and use both the spectral and temporal information given in the COHERENT data release [20]. In particular, as already shown in Refs. [10, 16], the combined spectral and temporal information of the COHERENT data allows us a better determination of the different interactions of ν_e and ν_μ than the spectral data alone, which are used in some analyses, or the total number of event data, which is used in the simplest analyses. This is due to the fact that in the Oak Ridge Spallation Neutron Source muon neutrinos are produced from π^+ decays at rest ($\pi^+ \rightarrow \mu^+ + \nu_\mu$) and arrive at the COHERENT detector as a prompt monochromatic signal with energy $(m_\pi^2 - m_\mu^2)/2m_\pi \simeq 29.8$ MeV, within about $1.5 \mu\text{s}$ after protons-on-target. On the other hand, muon antineutrinos and electron neutrinos are produced by μ^+ decays at rest ($\mu^+ \rightarrow e^+ + \nu_e + \bar{\nu}_\mu$) and arrive at the detector with continuous spectra extending up to $(m_\mu - m_e)/2 \simeq 52.8$ MeV in a longer time interval of about $10 \mu\text{s}$ after protons-on-target.

Since previous studies that obtained the constraints on NSI assuming interactions with either up or down quarks did not consider the complete spectral and temporal information of the COHERENT data and used the old quenching factor in Ref. [1], we present also the updated values of these constraints. This is particularly interesting for testing the LMA-Dark [21] fit of solar neutrino data [11].

Finally, we also present the constraints on each individual NSI parameter considered as the only non-vanishing one. This is the simplest approach for the analysis of the data and has been adopted by some authors. Although it is a very special case, it is physically possible if for some reason one of the NSI parameters is much larger than the other ones, whose effects are negligible in the analysis of the COHERENT data.

The plan of the paper is as follows. In Section II we review the contribution of NSI to coherent neutrino-nucleus elastic scattering, setting our conventions and notation. In Sections III we present the general constraints on NSI from the COHERENT data. In Section IV we present the constraints on NSI from the COHERENT data assuming only interactions with either up or down quarks. In Section V we present the constraints on each individual NSI parameter considered as the only effectively non-vanishing one. At the end, in Section VI we summarize our results.

* carlo.giunti@to.infn.it

II. NSI IN CE ν NS

We consider neutral-current neutrino non-standard interactions generated by a heavy mediator and described by the effective four-fermion interaction Lagrangian (see the reviews in Refs [22–25])

$$\mathcal{L}_{\text{NSI}}^{\text{NC}} = -2\sqrt{2}G_{\text{F}} \sum_{\alpha,\beta=e,\mu,\tau} (\overline{\nu_{\alpha L}}\gamma^{\rho}\nu_{\beta L}) \sum_{f=u,d} \varepsilon_{\alpha\beta}^{fV} (\overline{f}\gamma_{\rho}f), \quad (1)$$

where G_{F} is the Fermi constant. The parameters $\varepsilon_{\alpha\beta}^{fV}$ describe the size of non-standard interactions relative to standard neutral-current weak interactions. From the hermiticity of the Lagrangian, we have $\varepsilon_{\alpha\beta}^{fV} = \varepsilon_{\beta\alpha}^{fV*}$.

The differential cross section for coherent elastic scattering of a ν_{α} with energy E and a nucleus \mathcal{N} with Z protons, N neutrons, and mass M , is given by (see Ref. [26])

$$\frac{d\sigma_{\nu_{\alpha}\text{-}\mathcal{N}}}{dT}(E, T) = \frac{G_{\text{F}}^2 M}{\pi} \left(1 - \frac{MT}{2E^2}\right) Q_{\alpha}^2, \quad (2)$$

where T is the nuclear recoil kinetic energy and

$$Q_{\alpha}^2 = [(g_{\text{V}}^p + 2\varepsilon_{\alpha\alpha}^{uV} + \varepsilon_{\alpha\alpha}^{dV}) Z F_{\text{Z}}(|\vec{q}|^2) + (g_{\text{V}}^n + \varepsilon_{\alpha\alpha}^{uV} + 2\varepsilon_{\alpha\alpha}^{dV}) N F_{\text{N}}(|\vec{q}|^2)]^2 + \sum_{\beta \neq \alpha} [(2\varepsilon_{\alpha\beta}^{uV} + \varepsilon_{\alpha\beta}^{dV}) Z F_{\text{Z}}(|\vec{q}|^2) + (\varepsilon_{\alpha\beta}^{uV} + 2\varepsilon_{\alpha\beta}^{dV}) N F_{\text{N}}(|\vec{q}|^2)]^2, \quad (3)$$

with

$$g_{\text{V}}^p = \frac{1}{2} - 2\sin^2\vartheta_W, \quad g_{\text{V}}^n = -\frac{1}{2}. \quad (4)$$

Here ϑ_W is the weak mixing angle, given by $\sin^2\vartheta_W = 0.23857 \pm 0.00005$ at low energies [27].

In Eq. (3), $F_{\text{Z}}(|\vec{q}|^2)$ and $F_{\text{N}}(|\vec{q}|^2)$ are, respectively, the form factors of the proton and neutron distributions in the nucleus, that depend on the three-momentum transfer $|\vec{q}| \simeq \sqrt{2MT}$. They are given by the Fourier transforms of the nuclear proton and neutron distributions and describe the loss of coherence for $|\vec{q}|R_p \gtrsim 1$ and $|\vec{q}|R_n \gtrsim 1$, where R_p and R_n are the corresponding rms radii. It has been shown in Ref. [5] that different parameterizations of the form factors are practically equivalent in the analysis of COHERENT data. Therefore, we consider only the Helm parameterization [28]

$$F(|\vec{q}|^2) = 3 \frac{j_1(|\vec{q}|R_0)}{|\vec{q}|R_0} e^{-|\vec{q}|^2 s^2/2}, \quad (5)$$

where $j_1(x) = \sin(x)/x^2 - \cos(x)/x$ is the spherical Bessel function of order one, $s = 0.9$ fm [29] is the surface thickness and R_0 is related to the rms radius R by $R^2 = 3R_0^2/5 + 3s^2$. For the rms radii of the proton distributions of ^{133}Cs and ^{127}I we adopt the values determined with high accuracy from muonic atom spectroscopy [30]:

$$R_p(^{133}\text{Cs}) = 4.804 \text{ fm}, \quad R_p(^{127}\text{I}) = 4.749 \text{ fm}. \quad (6)$$

On the other hand, there is no separate measurement of the rms radii of the neutron distributions of ^{133}Cs and ^{127}I . The average neutron rms radius of CsI has been obtained from the COHERENT data assuming the absence of non-standard effects [5–10]. Taking into account also atomic parity violation (APV) experimental results [10, 18], the most precise determination of the average neutron rms radius of CsI from experimental data is [10]

$$R_n = 5.04 \pm 0.31 \text{ fm}. \quad (7)$$

Taking into account the uncertainties, this value is compatible with the predictions of nuclear models (see Table I in Ref. [5]). Since there are already ten NSI parameters to be determined by the analysis of the COHERENT data, it is practically advantageous to consider fixed values of the neutron rms radii of ^{133}Cs and ^{127}I , instead of considering them free as in Refs. [10, 16], where a smaller number of other parameters have been constrained. Hence, we adopt the values

$$R_n(^{133}\text{Cs}) = 5.01 \text{ fm}, \quad R_n(^{127}\text{I}) = 4.94 \text{ fm}, \quad (8)$$

obtained with the relativistic mean field (RMF) NL-Z2 [31] nuclear model calculation in Ref. [5], that are in good agreement with the average value (7). We take into account the form factor uncertainties with a 5% contribution to σ_{α_c} in the least-square functions (12) and (13), following the COHERENT prescription [1].

One can note that the NSI contributions of up and down quarks can cancel in Q_α^2 . A total cancellation happens for

$$\left[2 + \frac{N}{Z} \frac{F_N(|\vec{q}|^2)}{F_Z(|\vec{q}|^2)}\right] \varepsilon_{\alpha\beta}^{uV} + \left[1 + 2 \frac{N}{Z} \frac{F_N(|\vec{q}|^2)}{F_Z(|\vec{q}|^2)}\right] \varepsilon_{\alpha\beta}^{dV} = 0. \quad (9)$$

However, in practice only a partial cancellation is possible, because: 1) the ratio $F_N(|\vec{q}|^2)/F_Z(|\vec{q}|^2)$ depends on $|\vec{q}|^2$; 2) in the scattering on different nuclei, as ^{133}Cs and ^{127}I in the case of the COHERENT experiment, Z and N (and the corresponding form factors) are different. Nevertheless, since the proton and neutron form factors are not very different for a heavy nucleus and in the COHERENT case of scattering on CsI $(N/Z)_{^{133}\text{Cs}} \simeq 1.418$ is not very different of $(N/Z)_{^{127}\text{I}} \simeq 1.396$, the cancellation can be strong. This means that in practice coherent elastic neutrino-nucleus scattering is not sensitive to small values of the NSI couplings to u and d quarks if they are both considered as free parameters. As we will see in Section III, there is only a sensitivity to very large values of the NSI couplings to u and d quarks, for which the residuals of the cancellations are significant.

Considering $(N/Z)_{^{133}\text{Cs}} \simeq (N/Z)_{^{127}\text{I}} \simeq 1.4$ and neglecting the form factors, the cancellation relation (9) becomes

$$\varepsilon_{\alpha\beta}^{dV} \simeq -\frac{3.4}{3.8} \varepsilon_{\alpha\beta}^{uV} \simeq -0.89 \varepsilon_{\alpha\beta}^{uV}. \quad (10)$$

We will see in Section III that the allowed regions of the NSI parameters obtained from COHERENT data have a slope close to that in Eq. (10) and lie close to the corresponding line. This means that there is no indication of a significant NSI signal in the COHERENT data, taking into account the uncertainties.

From Eq. (10) one can see that the cancellation between the u and d couplings occurs when one is almost equal to the opposite of the other. This means that the COHERENT data are practically not sensitive to small values of the difference between $\varepsilon_{\alpha\beta}^{uV}$ and $\varepsilon_{\alpha\beta}^{dV}$, but can probe small values of linear combinations of $\varepsilon_{\alpha\beta}^{uV}$ and $\varepsilon_{\alpha\beta}^{dV}$ that are proportional to a value close to their average. Hence, in Section III we present also the constraints on the up-down averages

$$\bar{\varepsilon}_{\alpha\beta}^V = \frac{1}{2} (\varepsilon_{\alpha\beta}^{uV} + \varepsilon_{\alpha\beta}^{dV}). \quad (11)$$

III. GENERAL COHERENT CONSTRAINTS ON NSI

We performed two analyses of the COHERENT data: one of the spectral data only, and one of the joint spectral and temporal data. In this way we can evidence the improvements obtained by adding the temporal information, that has been previously used only in Refs. [10, 16, 17].

For the analysis of the COHERENT spectral data only, we considered the least-squares function

$$\chi_S^2 = \sum_{i=4}^{15} \left(\frac{N_i^{\text{exp}} - (1 + \alpha_c) N_i^{\text{th}} - (1 + \beta_c) B_i}{\sigma_i} \right)^2 + \left(\frac{\alpha_c}{\sigma_{\alpha_c}} \right)^2 + \left(\frac{\beta_c}{\sigma_{\beta_c}} \right)^2 + \left(\frac{\eta_c - 1}{\sigma_{\eta_c}} \right)^2. \quad (12)$$

Here, for each energy bin i , N_i^{exp} is the experimental event number, N_i^{th} is the theoretical event number that depends on the NSI parameters through the cross section (2), B_i is the estimated number of background events, and σ_i is the statistical uncertainty. We considered only the 12 energy bins from $i = 4$ to $i = 15$ of the COHERENT spectrum, because they cover the recoil kinetic energy of the new Chicago-3 quenching factor measurement [19], where the value of the quenching factor and its uncertainties are more reliable. In Eq. (12), α_c , β_c , and η_c are nuisance parameters which quantify, respectively, the systematic uncertainties of the signal rate, of the background rate, and of the quenching factor, with corresponding standard deviations $\sigma_{\alpha_c} = 0.12$, $\sigma_{\beta_c} = 0.25$ [1], and $\sigma_{\eta_c} = 0.05$ [19]. The value of σ_{α_c} has been obtained by summing in quadrature a 5% signal acceptance uncertainty, a 5% neutron form factor uncertainty, and a 10% neutron flux uncertainty, estimated by the COHERENT collaboration [1].

For the analysis of the joint COHERENT spectral and temporal data, we considered the least-squares function

$$\begin{aligned} \chi_{\text{ST}}^2 = 2 \sum_{i=4}^{15} \sum_{j=1}^{12} & \left[(1 + \alpha_c) N_{ij}^{\text{th}} + (1 + \beta_c) B_{ij} + (1 + \gamma_c) N_{ij}^{\text{bck}} - N_{ij}^{\text{C}} \right. \\ & \left. + N_{ij}^{\text{C}} \ln \left(\frac{N_{ij}^{\text{C}}}{(1 + \alpha_c) N_{ij}^{\text{th}} + (1 + \beta_c) B_{ij} + (1 + \gamma_c) N_{ij}^{\text{bck}}} \right) \right] \\ & + \left(\frac{\alpha_c}{\sigma_{\alpha_c}} \right)^2 + \left(\frac{\beta_c}{\sigma_{\beta_c}} \right)^2 + \left(\frac{\gamma_c}{\sigma_{\gamma_c}} \right)^2 + \left(\frac{\eta_c - 1}{\sigma_{\eta_c}} \right)^2, \end{aligned} \quad (13)$$

that allows us to take into account time-energy bins with few or zero events. In Eq. (13), i is the index of the energy bins, j is the index of the time bins, N_{ij}^{th} are the theoretical predictions that depend on the NSI parameters, N_{ij}^{C} are the coincidence (C) data, which contain signal and background events, B_{ij} are the estimated neutron-induced backgrounds, and N_{ij}^{bck} are the estimated backgrounds obtained from the anti-coincidence (AC) data given in the COHERENT data release [20]. The nuisance parameters α_c , β_c , and η_c are the same as in the least-square function in Eq. (12), that we used in the analysis of the time-integrated COHERENT data. The additional nuisance parameter γ_c and its uncertainty $\sigma_{\gamma_c} = 0.05$ quantify the systematic uncertainty of the background estimated from the AC data.

The general marginalized constraints on the NSI parameters obtained with the analyses of the spectral and the joint spectral and temporal COHERENT data are listed in Table I. Note that the bounds on the off-diagonal NSI parameters are given only for their absolute values, because a change in sign or phase does not have any effect in the upper bounds, as a consequence of the structure of Q_α^2 in Eq. (3).

From Table I, one can see that, as explained in Section II, the marginalized bounds on the individual NSI parameters $\varepsilon_{\alpha\beta}^{uV}$ and $\varepsilon_{\alpha\beta}^{dV}$ are very weak, because of the possible cancellations of their effects. On the other hand, the up-down averages $\bar{\varepsilon}_{\alpha\beta}^V$ in Eq. (11) are relatively well constrained, with upper values smaller or close to unity for reasonable values of the confidence level. However, these constraints are larger than may be expected, for example from the analysis in Ref. [12] that found the 90% CL bounds $-0.16 \leq \bar{\varepsilon}_{ee}^V \leq 0.33$ and $-0.11 \leq \bar{\varepsilon}_{\mu\mu}^V \leq 0.26$. The reason why the constraints on the averages $\bar{\varepsilon}_{\alpha\beta}^V$ cannot be so tight is that these averages do not satisfy well the cancellation constraint in Eq. (10), especially when the individual up and down NSI parameters are large and with opposite signs. Therefore, we consider also the optimal up-down linear combinations

$$\tilde{\varepsilon}_{\alpha\beta}^V = \frac{3.4 \varepsilon_{\alpha\beta}^{uV} + 3.8 \varepsilon_{\alpha\beta}^{dV}}{7.2}. \quad (14)$$

Table I shows that the constraints for these optimal up-down linear combinations are strong. In the joint COHERENT spectral and temporal data analysis the absolute values of all the optimal up-down linear combinations of NSI parameters are smaller than 0.35 at 3σ . The larger values of the constraints on the averages $\bar{\varepsilon}_{\alpha\beta}^V$ are due to the fact that $\varepsilon_{\alpha\beta}^{uV}$ and $\varepsilon_{\alpha\beta}^{dV}$ can be large and opposite yielding a very small value of $\tilde{\varepsilon}_{\alpha\beta}^V$ that corresponds to a much larger value of $\bar{\varepsilon}_{\alpha\beta}^V$. For example, if we consider $\varepsilon_{ee}^{uV} = 10$, that is allowed within 1σ by the limits in Table I, we have $\varepsilon_{ee}^{uV} = 0.2$, that is allowed within 1σ , for $\varepsilon_{ee}^{dV} = -8.6$, that is also allowed within 1σ . In this case $\bar{\varepsilon}_{ee}^V = 0.7$ and this value must be allowed within 1σ , in agreement with Table I and contrary to the limits in Ref. [12].

It is clear from Table I that the analysis of the joint COHERENT spectral and temporal data is more powerful in constraining the NSI parameters than the analysis of the spectral data only. Therefore, in the rest of this Section we discuss only the results of the joint spectral and temporal data analysis.

Figures 1–5 show the allowed regions in the planes $(\varepsilon_{\alpha\beta}^{uV}, \varepsilon_{\alpha\beta}^{dV})$ with $\alpha = e, \mu$ and $\beta = e, \mu, \tau$. For the off-diagonal NSI parameters, the allowed regions are marginalized in the real planes. From these figures, one can see that all the allowed regions are approximately parallel to the line in Eq. (10), in agreement with the expectation. The enlargements in the right panels show that the preferred values of the NSI parameters are close to the approximate cancellation line (10), indicating that there is no indication of NSI effects within the uncertainties.

Near the origin the boundaries of the 1σ , 2σ , and 3σ allowed regions can be parameterized with the lines

$$\varepsilon_{\alpha\beta}^{dV} = a \varepsilon_{\alpha\beta}^{uV} + b, \quad (15)$$

with the values of the parameters a and b given in Table II. One can see that the slopes a are all very close to the one in Eq. (10), as expected.

Figure 6 shows the marginal allowed regions in different planes of the up-down average NSI parameters $\bar{\varepsilon}_{\alpha\beta}^V$ in Eq. (11), that are relatively well constrained by the COHERENT data. However, as shown in Table I and Figure 7, the strongest constraints are obtained for the optimal up-down linear combinations $\tilde{\varepsilon}_{\alpha\beta}^V$ in Eq. (14).

IV. COHERENT CONSTRAINTS ON NSI WITH EITHER UP OR DOWN QUARKS

In this Section we consider the possibility that neutrino NSI with nuclei are dominated by either up or down quarks, with the subdominant quark NSI having negligible effects. The results of the analysis assuming interactions with up quark only are given in Table III, and those obtained assuming interactions with down quark only are given in Table IV. From these tables one can see that with these assumptions the NSI parameters are well determined to be smaller than one at more than 3σ in both the spectral and the joint spectral and temporal analyses. Since the joint spectral and temporal analysis is more restrictive, we present only the corresponding correlated allowed regions in different planes of the NSI parameters in Figure 8 for interactions with up quarks only and in Figure 9 for interactions with down quarks only.

Figures 8 and 9 show the comparison of the COHERENT allowed regions in the $(\varepsilon_{ee}^{uV}, \varepsilon_{\mu\mu}^{uV})$ and $(\varepsilon_{ee}^{dV}, \varepsilon_{\mu\mu}^{dV})$ planes, respectively, with the solar LMA-Dark [21] allowed regions reported in Ref. [11]. One can see that the allowed regions are incompatible at more than 3σ , disfavoring the LMA-Dark fit of solar neutrino data more than in Ref. [11], where the analysis of the COHERENT data was performed considering only the total number of events.

Combining the χ^2 's of the analyses of COHERENT spectral data with the marginal $\Delta\chi^2$'s of the LMA-Dark and LMA fits of solar neutrino data in Fig. 1 of Ref. [11], we found a χ_{\min}^2 difference between LMA-Dark and LMA of 24.5 and 46.5, respectively, for NSI with up and down quark. Therefore, LMA-Dark is excluded at 4.9σ and 6.8σ , respectively, for NSI with up and down quark, for one degree of freedom. These exclusions are already much stronger than the 3.1σ and 3.6σ obtained in Ref. [11]. We further improved the comparison between LMA-Dark and LMA by considering the COHERENT spectral and temporal data, that lead to the exclusion of LMA-Dark at 5.6σ ($\Delta\chi_{\min}^2 = 31.3$) and 7.2σ ($\Delta\chi_{\min}^2 = 52.6$), respectively, for NSI with up and down quark.

One can note that our allowed region from COHERENT data in the $(\varepsilon_{ee}^{uV}, \varepsilon_{\mu\mu}^{uV})$ plane has a different shape than that in Figure 2 of Ref. [11], that has a hole around about $(0.2, 0.2)$. The only explanation that we found of this difference is that in Ref. [11], in spite of the statements in the text, the allowed region was not calculated marginalizing over the remaining off-diagonal NSI parameters of the interaction with up quarks. Indeed, a hole in the allowed region of $(\varepsilon_{ee}^{uV}, \varepsilon_{\mu\mu}^{uV})$ appears around about $(0.2, 0.2)$ if only the first line in Eq. (3) is considered and corresponds to its suppression. Neglecting $g_V^p \simeq 0.023$ and the form factors, for $\varepsilon_{\alpha\alpha}^{dV} = 0$ the first line in Eq. (3) vanishes for

$$\varepsilon_{\alpha\alpha}^{uV} \simeq \frac{N}{2(2Z + N)} \simeq 0.21 \quad (\alpha = e, \mu), \quad (16)$$

considering the average CsI values $Z = 54$ and $N = 76$. If one does not consider the effects of the off-diagonal NSI parameters of the interaction with up quarks in the second line of Eq. (3) the cross section is suppressed around $(\varepsilon_{ee}^{uV}, \varepsilon_{\mu\mu}^{uV}) \simeq (0.2, 0.2)$ generating a hole in the allowed region. However, appropriate values of the off-diagonal NSI parameters of the interaction with up quarks can compensate the suppression of the first line in Eq. (3), filling the hole. That is why our allowed region in Figure 8 has no hole.

As a further check, we present in the left panel of Figure 10 the allowed region in the $(\varepsilon_{ee}^{uV}, \varepsilon_{\mu\mu}^{uV})$ plane that we obtained assuming that only these two NSI parameters are non-vanishing and fitting the COHERENT spectral data alone. One can see that there is a hole around $(0.2, 0.2)$ and the shape is similar to that in Ref. [11]. The left panel in Figure 11 shows that the allowed region reduces significantly in the analysis of the joint COHERENT spectral and temporal data, increasing the tension with the LMA-Dark fit of solar neutrino data.

The allowed region in the $(\varepsilon_{ee}^{uV}, \varepsilon_{\mu\mu}^{uV})$ plane assuming only these two non-vanishing NSI parameters was obtained also in Ref. [9] by fitting the COHERENT spectral data. Our allowed region in the left panel of Figure 10 is more stringent than that in the right panel of Fig. 7 of Ref. [9], probably because in Ref. [9] the quenching factor was approximated with a constant, whereas we implemented the T -dependent quenching factor function in Ref. [19].

For completeness, we present in the right panels of Figure 10 and 11 also the allowed regions in the $(\varepsilon_{ee}^{dV}, \varepsilon_{\mu\mu}^{dV})$ plane that we obtained assuming that only these two NSI parameters are non-vanishing. In this case the hole corresponding to the suppression of the first line in Eq. (3) occurs for

$$\varepsilon_{\alpha\alpha}^{dV} \simeq \frac{N}{2(Z + 2N)} \simeq 0.18 \quad (\alpha = e, \mu), \quad (17)$$

considering the average CsI values $Z = 54$ and $N = 76$. The figures show also the strong tension with the LMA-Dark fit of solar neutrino data.

V. COHERENT CONSTRAINTS ON DOMINANT INDIVIDUAL NSI PARAMETERS

In this Section we present the results of the analyses of COHERENT data assuming that only one of the NSI parameters is dominant and the others have negligible effects. The allowed intervals for each parameter are listed in

Table V. Figure 12 shows the $\Delta\chi^2 = \chi^2 - \chi_{\min}^2$ for each parameter. One can see that for the diagonal NSI parameters and some confidence levels there are disconnected allowed intervals, because the $\Delta\chi^2$ is not parabolic, but has a local central maximum. This occurs for the same reason of the hole in the two-dimensional plots in Figures 10 and 11, because there is a cancellation in the first line of Eq. (3) that suppresses the cross section and gives a bad fit of the data. Indeed, the local central maximum occurs at a value of about 0.2, in agreement with Eqs. (16) and (17).

Table V and Figure 12 show that the individual NSI parameters are better determined with the analysis of the joint COHERENT spectral and temporal data than with the analysis of the spectral data alone. The resulting bounds are more stringent than those obtained recently in Refs. [8, 9].

In particular, the diagonal ν_μ NSI parameters $\varepsilon_{\mu\mu}^{uV}$ and $\varepsilon_{\mu\mu}^{dV}$ are well constrained in two disconnected intervals at 3σ with the joint spectral and temporal analysis. In general, the constraints on the ν_μ NSI parameters are more stringent than those on the ν_e NSI parameters because there are two ν_μ fluxes, one from π^+ decay and one, of $\bar{\nu}_\mu$, from μ^+ decay, whereas there is only one flux of ν_e from μ^+ decay. One can also note that $\varepsilon_{e\mu}^{uV}$ and $\varepsilon_{e\mu}^{dV}$ are more constrained than the other off-diagonal NSI parameters, because they contribute to all the interactions of ν_μ , $\bar{\nu}_\mu$, and ν_e . The less constrained off-diagonal NSI parameters are $\varepsilon_{e\tau}^{uV}$ and $\varepsilon_{e\tau}^{dV}$, that contribute only to the interactions of the ν_e flux.

VI. CONCLUSIONS

In this work we performed a systematic study of the constraints on neutrino neutral-current non-standard interactions that can be obtained from the analysis of the COHERENT spectral and temporal data. We have shown that the joint analysis of the COHERENT spectral and temporal data gives more information on the NSI parameters than the analysis of the COHERENT spectral data alone. This is a general feature for quantities that depend on the neutrino flavor, as already emphasized in Refs. [10, 16].

First, we considered for the first time the general case in which all the ten neutral-current NSI parameters are considered as free. We have shown that in this case the analysis of the COHERENT data give very weak constraints the NSI parameters, because the contributions of the NSI parameters with up and down quarks can almost entirely cancel each other. The up-down average parameters in Eq. (11) are relatively well constrained, but the strongest constraints are obtained for the optimal up-down linear combination of NSI parameters in Eq. (14).

We also considered the case in which there are only NSI with either up or down quarks, that was considered in Ref. [11] in order to test the LMA-Dark fit of solar neutrino data. In this case, we obtained very stringent constraints on the NSI parameters, that exclude LMA-Dark at 5.6σ and 7.2σ respectively, for NSI with up and down quark. These exclusions are much stronger than the 3.1σ and 3.6σ obtained in Ref. [11].

We finally considered also the case of only one dominant NSI parameter, assuming that the effects of the others is negligible. This is the simplest analysis that has been performed recently also by other authors [8, 9]. We obtained more stringent constraints on each individual NSI parameter through the joint analysis of the COHERENT spectral and temporal data.

-
- [1] D. Akimov *et al.* (COHERENT), *Science* **357**, 1123 (2017), arXiv:1708.01294 [nucl-ex].
 - [2] D. Z. Freedman, *Phys. Rev.* **D9**, 1389 (1974).
 - [3] D. Z. Freedman, D. N. Schramm, and D. L. Tubbs, *Ann. Rev. Nucl. Part. Sci.* **27**, 167 (1977).
 - [4] A. Drukier and L. Stodolsky, *Phys. Rev.* **D30**, 2295 (1984).
 - [5] M. Cadeddu, C. Giunti, Y. F. Li, and Y. Y. Zhang, *Phys.Rev.Lett.* **120**, 072501 (2018), arXiv:1710.02730 [hep-ph].
 - [6] D. K. Papoulias, T. S. Kosmas, R. Sahu, V. K. B. Kota, and M. Hota, arXiv:1903.03722 [hep-ph].
 - [7] X.-R. Huang and L.-W. Chen, arXiv:1902.07625 [hep-ph].
 - [8] D. K. Papoulias, arXiv:1907.11644 [hep-ph].
 - [9] A. N. Khan and W. Rodejohann, arXiv:1907.12444 [hep-ph].
 - [10] M. Cadeddu, F. Dordei, C. Giunti, Y. Li, and Y. Zhang, arXiv:1908.06045 [hep-ph].
 - [11] P. Coloma, M. C. Gonzalez-Garcia, M. Maltoni, and T. Schwetz, *Phys.Rev.* **D96**, 115007 (2017), arXiv:1708.02899 [hep-ph].
 - [12] J. Liao and D. Marfatia, *Phys.Lett.* **B775**, 54 (2017), arXiv:1708.04255 [hep-ph].
 - [13] D. K. Papoulias and T. S. Kosmas, *Phys.Rev.* **D97**, 033003 (2018), arXiv:1711.09773 [hep-ph].
 - [14] P. B. Denton, Y. Farzan, and I. M. Shoemaker, *JHEP* **1807**, 037 (2018), arXiv:1804.03660 [hep-ph].
 - [15] D. Aristizabal Sierra, V. De Romeri, and N. Rojas, *Phys.Rev.* **D98**, 075018 (2018), arXiv:1806.07424 [hep-ph].
 - [16] M. Cadeddu, C. Giunti, K. Kouzakov, Y. F. Li, A. Studenikin, and Y. Y. Zhang, *Phys.Rev.* **D98**, 113010 (2018), arXiv:1810.05606 [hep-ph].
 - [17] B. Dutta, S. Liao, S. Sinha, and L. E. Strigari, *Phys.Rev.Lett.* **123**, 061801 (2019), arXiv:1903.10666 [hep-ph].
 - [18] M. Cadeddu and F. Dordei, *Phys.Rev.* **D99**, 033010 (2019), arXiv:1808.10202 [hep-ph].

- [19] J. I. Collar, A. R. L. Kavner, and C. M. Lewis, Phys.Rev. **D100**, 033003 (2019), arXiv:1907.04828 [nucl-ex].
[20] D. Akimov *et al.* (COHERENT), arXiv:1804.09459 [nucl-ex].
[21] O. G. Miranda, M. A. Tortola, and J. W. F. Valle, JHEP **10**, 008 (2006), hep-ph/0406280.
[22] T. Ohlsson, Rept.Prog.Phys. **76**, 044201 (2013), arXiv:1209.2710 [hep-ph].
[23] O. Miranda and H. Nunokawa, New J. Phys. **17**, 095002 (2015), arXiv:1505.06254 [hep-ph].
[24] Y. Farzan and M. Tortola, Front.in Phys. **6**, 10 (2018), arXiv:1710.09360 [hep-ph].
[25] P. S. B. Dev *et al.*, arXiv:1907.00991 [hep-ph].
[26] J. Barranco, O. G. Miranda, and T. I. Rashba, JHEP **0512**, 021 (2005), hep-ph/0508299.
[27] M. Tanabashi *et al.* (Particle Data Group), Phys. Rev. **D98**, 030001 (2018).
[28] R. H. Helm, Phys. Rev. **104**, 1466 (1956).
[29] J. Friedrich and N. Voegler, Nucl. Phys. **A373**, 192 (1982).
[30] G. Fricke, C. Bernhardt, K. Heilig, L. A. Schaller, L. Schellenberg, E. B. Shera, and C. W. de Jager, Atom. Data Nucl. Data Tabl. **60**, 177 (1995).
[31] M. Bender, K. Rutz, P. G. Reinhard, J. A. Maruhn, and W. Greiner, Phys. Rev. **C60**, 034304 (1999), nucl-th/9906030 [nucl-th].

	Spectrum				Spectrum and Time			
	Best Fit	1 σ	2 σ	3 σ	Best Fit	1 σ	2 σ	3 σ
ε_{ee}^{uV}	0	-29 \div 29	-38 \div 39	-47 \div 47	0	-15 \div 15	-27 \div 26	-35 \div 35
ε_{ee}^{dV}	0	-26 \div 26	-35 \div 35	-42 \div 43	0	-13 \div 14	-24 \div 24	-31 \div 32
$\varepsilon_{\mu\mu}^{uV}$	0	-25 \div 25	-32 \div 32	-39 \div 40	0	-11 \div 11	-19 \div 19	-26 \div 25
$\varepsilon_{\mu\mu}^{dV}$	0	-23 \div 23	-29 \div 30	-36 \div 36	0	-10 \div 10	-17 \div 18	-22 \div 24
$ \varepsilon_{e\mu}^{uV} $	0	< 19	< 25	< 30	0	< 9	< 16	< 21
$ \varepsilon_{e\mu}^{dV} $	0	< 17	< 22	< 27	0	< 8	< 14	< 19
$ \varepsilon_{e\tau}^{uV} $	0	< 29	< 38	< 47	0	< 15	< 26	< 35
$ \varepsilon_{e\tau}^{dV} $	0	< 26	< 35	< 43	0	< 14	< 24	< 31
$ \varepsilon_{\mu\tau}^{uV} $	0	< 25	< 32	< 39	0	< 11	< 19	< 25
$ \varepsilon_{\mu\tau}^{dV} $	0	< 23	< 29	< 36	0	< 10	< 17	< 23
$\tilde{\varepsilon}_{ee}^V$	0.1	-1.2 \div 1.4	-1.7 \div 1.9	-2.1 \div 2.2	0.1	-0.7 \div 0.8	-1.1 \div 1.3	-1.6 \div 1.7
$\tilde{\varepsilon}_{\mu\mu}^V$	0	-1.0 \div 1.2	-1.3 \div 1.5	-1.7 \div 1.9	0.1	-0.4 \div 0.6	-0.8 \div 1.0	-1.1 \div 1.3
$ \tilde{\varepsilon}_{e\mu}^V $	0.1	< 0.9	< 1.1	< 1.4	0.1	< 0.4	< 0.7	< 1.0
$ \tilde{\varepsilon}_{e\tau}^V $	0.2	< 1.3	< 1.8	< 2.2	0.1	< 0.8	< 1.2	< 1.6
$ \tilde{\varepsilon}_{\mu\tau}^V $	0.5	< 1.1	< 1.5	< 1.8	0.1	< 0.6	< 0.9	< 1.2
$\tilde{\varepsilon}_{ee}^V$	0.09	-0.17 \div 0.35	-0.23 \div 0.42	-0.29 \div 0.48	0.09	-0.01 \div 0.20	-0.10 \div 0.29	-0.17 \div 0.35
$\tilde{\varepsilon}_{\mu\mu}^V$	0.09	-0.15 \div 0.34	-0.20 \div 0.38	-0.24 \div 0.43	0.10	-0.04 \div 0.23	-0.08 \div 0.27	-0.11 \div 0.30
$ \tilde{\varepsilon}_{e\mu}^V $	0.04	< 0.18	< 0.22	< 0.25	0.01	< 0.10	< 0.14	< 0.17
$ \tilde{\varepsilon}_{e\tau}^V $	0.05	< 0.27	< 0.33	< 0.38	0.02	< 0.11	< 0.19	< 0.26
$ \tilde{\varepsilon}_{\mu\tau}^V $	0.13	< 0.24	< 0.30	< 0.34	0.06	< 0.13	< 0.17	< 0.21

TABLE I. General marginalized constraints on the NSI parameters obtained with the analyses of the spectral and the joint spectral and temporal COHERENT data.

		1 σ		2 σ		3 σ	
		<i>a</i>	<i>b</i>	<i>a</i>	<i>b</i>	<i>a</i>	<i>b</i>
$(\varepsilon_{ee}^{uV}, \varepsilon_{ee}^{dV})$	LB	-0.90	-0.02	-0.90	-0.10	-0.91	-0.15
	UB	-0.90	0.36	-0.90	0.43	-0.90	0.50
$(\varepsilon_{\mu\mu}^{uV}, \varepsilon_{\mu\mu}^{dV})$	LB	-0.90	-0.05	-0.91	-0.08	-0.91	-0.11
	UB	-0.92	0.41	-0.91	0.43	-0.92	0.47
$(\varepsilon_{e\mu}^{uV}, \varepsilon_{e\mu}^{dV})$	LB	-0.92	-0.17	-0.91	-0.20	-0.91	-0.24
	UB	-0.92	0.18	-0.91	0.21	-0.91	0.23
$(\varepsilon_{e\tau}^{uV}, \varepsilon_{e\tau}^{dV})$	LB	-0.91	-0.19	-0.91	-0.27	-0.91	-0.32
	UB	-0.92	0.19	-0.91	0.27	-0.90	0.32
$(\varepsilon_{\mu\tau}^{uV}, \varepsilon_{\mu\tau}^{dV})$	LB	-0.90	-0.22	-0.90	-0.26	-0.91	-0.29
	UB	-0.91	0.23	-0.91	0.26	-0.92	0.30

TABLE II. Values of the parameters a and b in Eq. (15) of the lower (LB) and upper (UB) boundaries of the allowed regions in the right panels of Figures 1–5.

	Spectrum				Spectrum and Time			
	Best Fit	1 σ	2 σ	3 σ	Best Fit	1 σ	2 σ	3 σ
ε_{ee}^{uV}	0.02	-0.18 \div 0.56	-0.23 \div 0.62	-0.28 \div 0.66	0.20	0.01 \div 0.38	-0.08 \div 0.47	-0.15 \div 0.54
$\varepsilon_{\mu\mu}^{uV}$	0.18	-0.08 \div 0.44	-0.13 \div 0.51	-0.17 \div 0.56	0.20	-0.06 \div 0.45	-0.10 \div 0.48	-0.13 \div 0.52
$ \varepsilon_{e\mu}^{uV} $	0.04	< 0.22	< 0.26	< 0.29	0.04	< 0.19	< 0.23	< 0.26
$ \varepsilon_{e\tau}^{uV} $	0.16	< 0.37	< 0.42	< 0.47	0.04	< 0.19	< 0.28	< 0.35
$ \varepsilon_{\mu\tau}^{uV} $	0.04	< 0.26	< 0.32	< 0.37	0.12	< 0.26	< 0.29	< 0.32

TABLE III. Marginalized constraints on the NSI parameters obtained with the analyses of the spectral and the joint spectral and temporal COHERENT data assuming NSI with the up quark only.

	Spectrum				Spectrum and Time			
	Best Fit	1 σ	2 σ	3 σ	Best Fit	1 σ	2 σ	3 σ
ε_{ee}^{dV}	0.17	-0.16 \div 0.52	-0.20 \div 0.56	-0.25 \div 0.60	0.18	0.01 \div 0.34	-0.07 \div 0.42	-0.14 \div 0.49
$\varepsilon_{\mu\mu}^{dV}$	0.17	-0.07 \div 0.41	-0.12 \div 0.47	-0.16 \div 0.51	0.18	-0.06 \div 0.41	-0.08 \div 0.44	-0.12 \div 0.47
$ \varepsilon_{e\mu}^{dV} $	0.04	< 0.20	< 0.23	< 0.26	0.04	< 0.17	< 0.21	< 0.24
$ \varepsilon_{e\tau}^{dV} $	0.16	< 0.34	< 0.38	< 0.43	0.04	< 0.17	< 0.25	< 0.31
$ \varepsilon_{\mu\tau}^{dV} $	0.04	< 0.24	< 0.30	< 0.33	0.11	< 0.23	< 0.26	< 0.29

TABLE IV. Marginalized constraints on the NSI parameters obtained with the analyses of the spectral and the joint spectral and temporal COHERENT data assuming NSI with the down quark only.

	Spectrum			Spectrum and Time		
	1σ	2σ	3σ	1σ	2σ	3σ
ε_{ee}^{uV}	$\begin{pmatrix} -0.09 \div 0.03 \\ 0.36 \div 0.48 \end{pmatrix}$	$\begin{pmatrix} -0.15 \div 0.17 \\ 0.23 \div 0.54 \end{pmatrix}$	$-0.21 \div 0.60$	$\begin{pmatrix} -0.02 \div 0.18 \\ 0.21 \div 0.41 \end{pmatrix}$	$-0.08 \div 0.47$	$-0.15 \div 0.53$
$\varepsilon_{\mu\mu}^{uV}$	$\begin{pmatrix} -0.06 \div 0.03 \\ 0.37 \div 0.44 \end{pmatrix}$	$\begin{pmatrix} -0.10 \div 0.08 \\ 0.31 \div 0.49 \end{pmatrix}$	$-0.15 \div 0.53$	$\begin{pmatrix} -0.03 \div 0.03 \\ 0.37 \div 0.42 \end{pmatrix}$	$\begin{pmatrix} -0.07 \div 0.06 \\ 0.33 \div 0.46 \end{pmatrix}$	$\begin{pmatrix} -0.11 \div 0.10 \\ 0.29 \div 0.49 \end{pmatrix}$
$ \varepsilon_{e\mu}^{uV} $	< 0.13	< 0.17	< 0.22	< 0.09	< 0.14	< 0.19
$ \varepsilon_{e\tau}^{uV} $	< 0.21	< 0.29	< 0.36	< 0.12	< 0.21	< 0.28
$ \varepsilon_{\mu\tau}^{uV} $	< 0.16	< 0.22	< 0.28	< 0.12	< 0.18	< 0.23
ε_{ee}^{dV}	$\begin{pmatrix} -0.09 \div 0.03 \\ 0.33 \div 0.43 \end{pmatrix}$	$\begin{pmatrix} -0.14 \div 0.15 \\ 0.21 \div 0.49 \end{pmatrix}$	$-0.19 \div 0.55$	$\begin{pmatrix} -0.02 \div 0.17 \\ 0.18 \div 0.37 \end{pmatrix}$	$-0.07 \div 0.43$	$-0.13 \div 0.48$
$\varepsilon_{\mu\mu}^{dV}$	$\begin{pmatrix} -0.05 \div 0.02 \\ 0.33 \div 0.40 \end{pmatrix}$	$\begin{pmatrix} -0.09 \div 0.07 \\ 0.28 \div 0.44 \end{pmatrix}$	$-0.13 \div 0.48$	$\begin{pmatrix} -0.03 \div 0.02 \\ 0.33 \div 0.38 \end{pmatrix}$	$\begin{pmatrix} -0.06 \div 0.05 \\ 0.30 \div 0.41 \end{pmatrix}$	$\begin{pmatrix} -0.09 \div 0.09 \\ 0.27 \div 0.45 \end{pmatrix}$
$ \varepsilon_{e\mu}^{dV} $	< 0.12	< 0.16	< 0.20	< 0.08	< 0.13	< 0.17
$ \varepsilon_{e\tau}^{dV} $	< 0.19	< 0.26	< 0.33	< 0.11	< 0.19	< 0.25
$ \varepsilon_{\mu\tau}^{dV} $	< 0.15	< 0.20	< 0.25	< 0.11	< 0.16	< 0.21

TABLE V. Allowed intervals for each of the NSI parameter assuming it to be the only non-vanishing one. Disconnected intervals are grouped in parentheses.

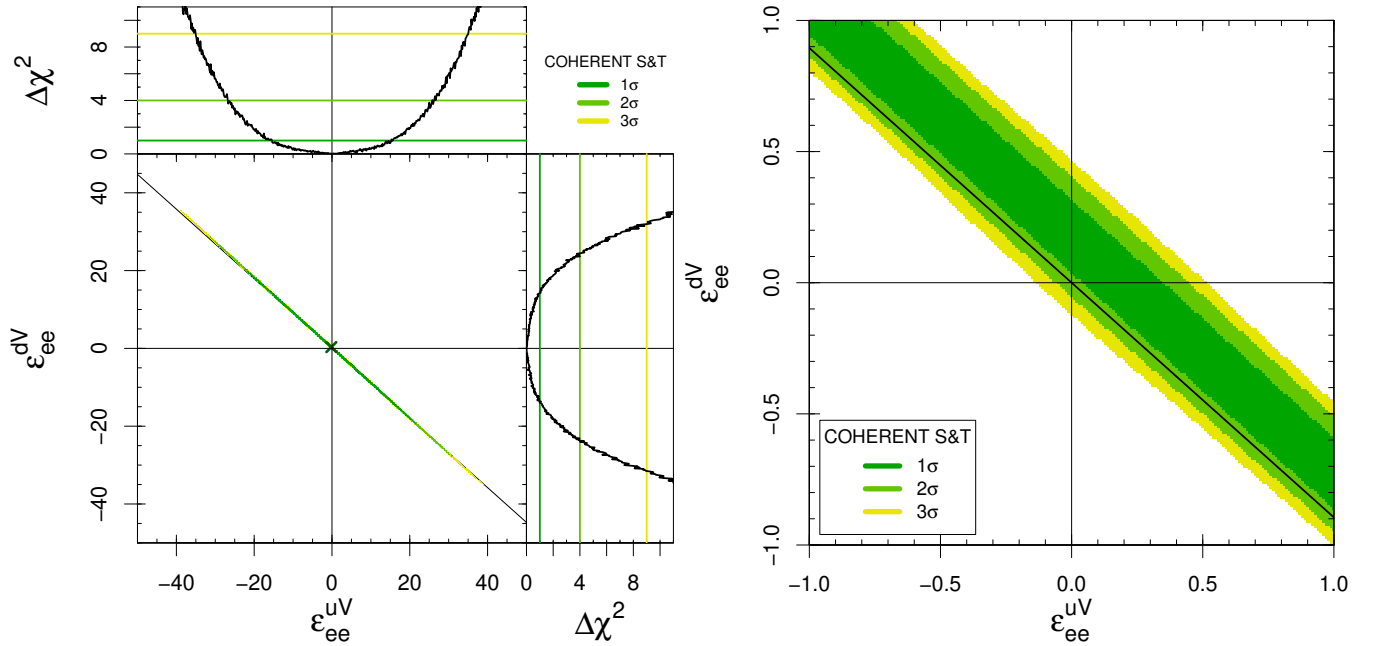


FIG. 1. Left panel: general marginalized allowed region in the $(\varepsilon_{ee}^{uV}, \varepsilon_{ee}^{dV})$ plane and marginal $\Delta\chi^2$'s obtained from the analysis of the joint COHERENT spectral and temporal (S&T) data. Right panel: enlargement of the area around the origin. The diagonal black lines represent the relation (10). The point indicates the best-fit values.

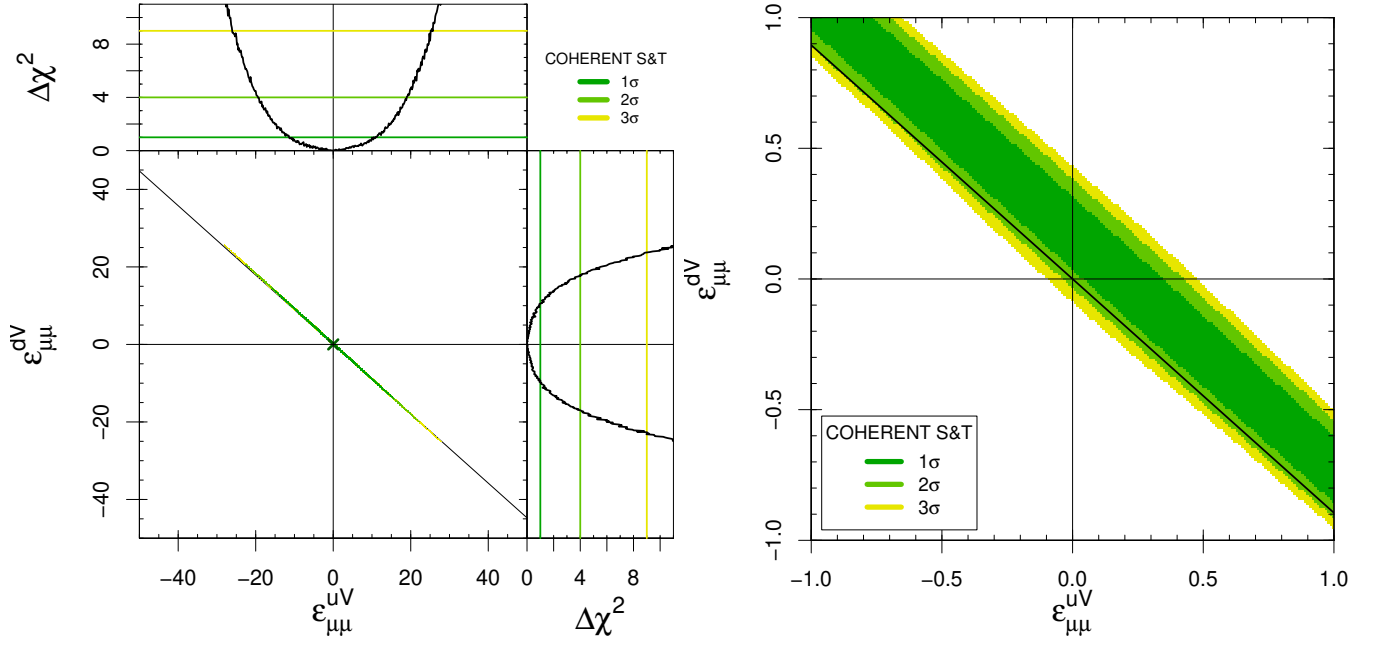


FIG. 2. Left panel: general marginalized allowed region in the $(\varepsilon_{\mu\mu}^{uV}, \varepsilon_{\mu\mu}^{dV})$ plane and marginal $\Delta\chi^2$'s obtained from the analysis of the joint COHERENT spectral and temporal (S&T) data. Right panel: enlargement of the area around the origin. The diagonal black lines represent the relation (10). The point indicates the best-fit values.

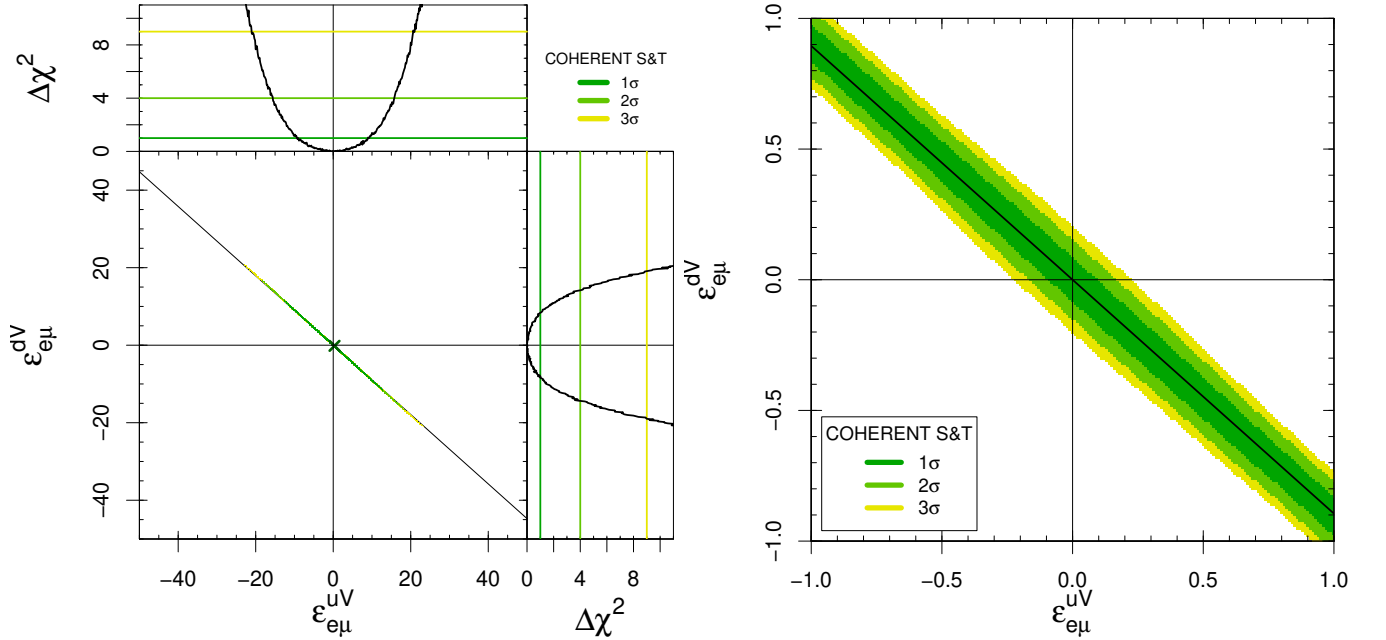


FIG. 3. Left panel: general marginalized allowed region in the real $(\varepsilon_{e\mu}^{uV}, \varepsilon_{e\mu}^{dV})$ plane and marginal $\Delta\chi^2$'s obtained from the analysis of the joint COHERENT spectral and temporal (S&T) data. Right panel: enlargement of the area around the origin. The diagonal black lines represent the relation (10). The point indicates the best-fit values.

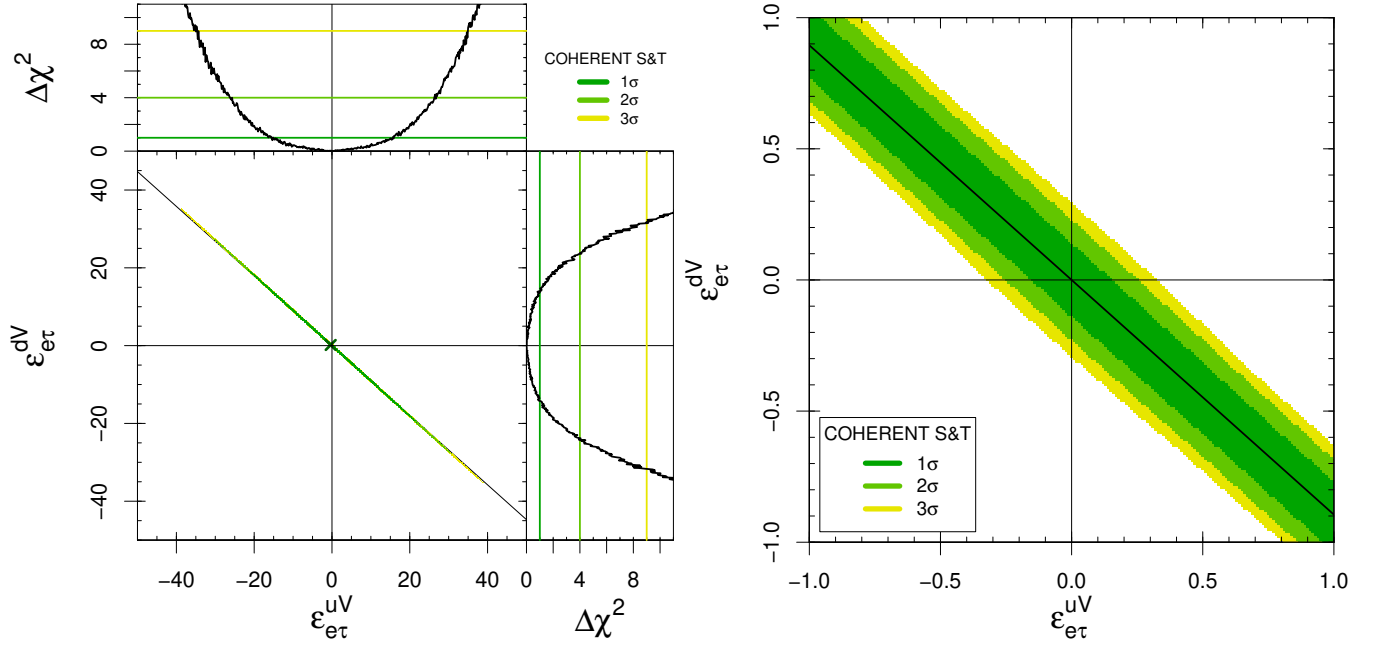


FIG. 4. Left panel: general marginalized allowed region in the real $(\epsilon_{e\tau}^{uV}, \epsilon_{e\tau}^{dV})$ plane and marginal $\Delta\chi^2$'s obtained from the analysis of the joint COHERENT spectral and temporal (S&T) data. Right panel: enlargement of the area around the origin. The diagonal black lines represent the relation (10). The point indicates the best-fit values.

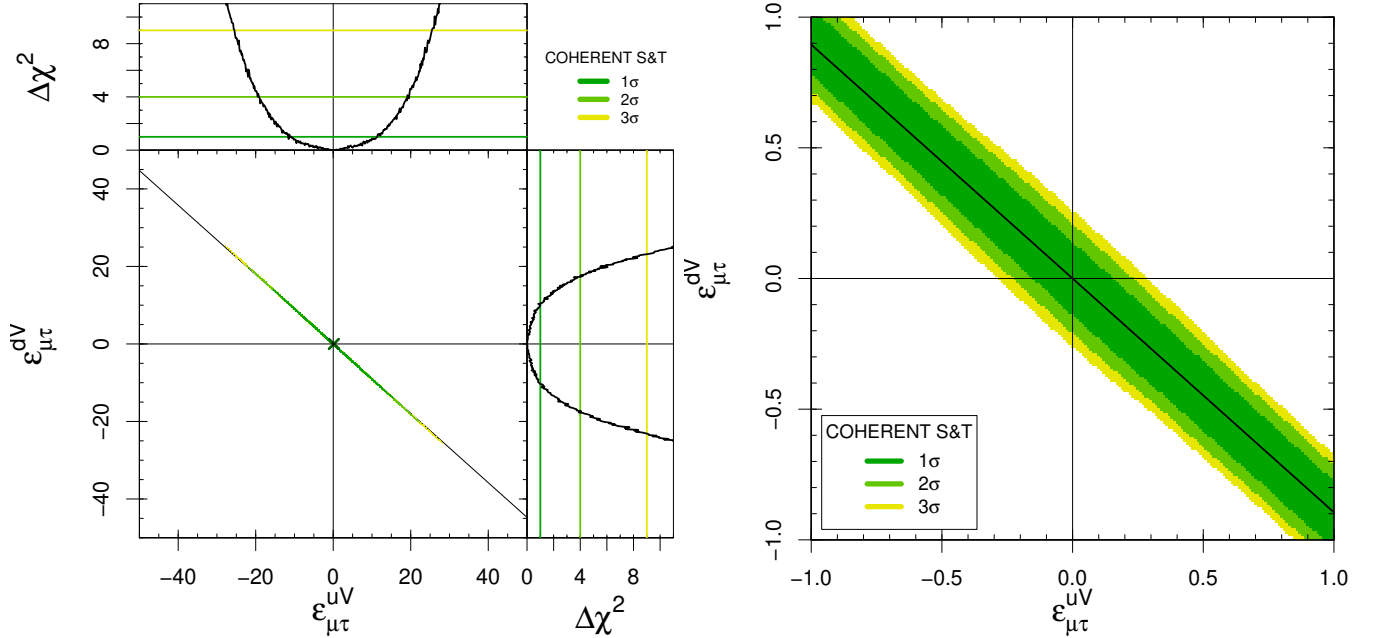


FIG. 5. Left panel: general marginalized allowed region in the real $(\epsilon_{\mu\tau}^{uV}, \epsilon_{\mu\tau}^{dV})$ plane and marginal $\Delta\chi^2$'s obtained from the analysis of the joint COHERENT spectral and temporal (S&T) data. Right panel: enlargement of the area around the origin. The diagonal black lines represent the relation (10). The point indicates the best-fit values.

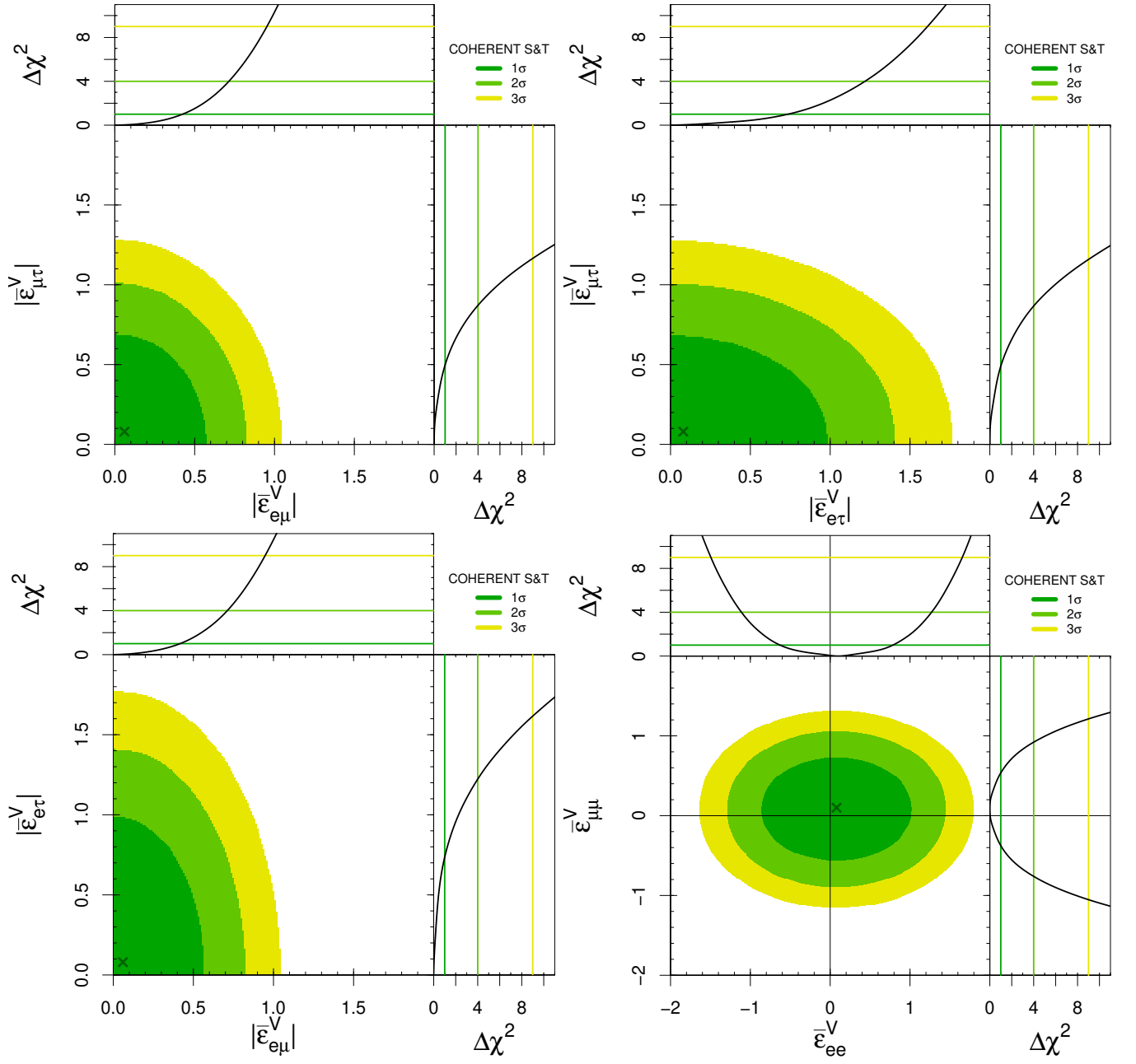


FIG. 6. General marginalized allowed regions in different planes of the up-down average NSI parameters (11) and marginal $\Delta\chi^2$'s obtained from the analysis of the joint COHERENT spectral and temporal (S&T) data. The points indicate the best-fit values.

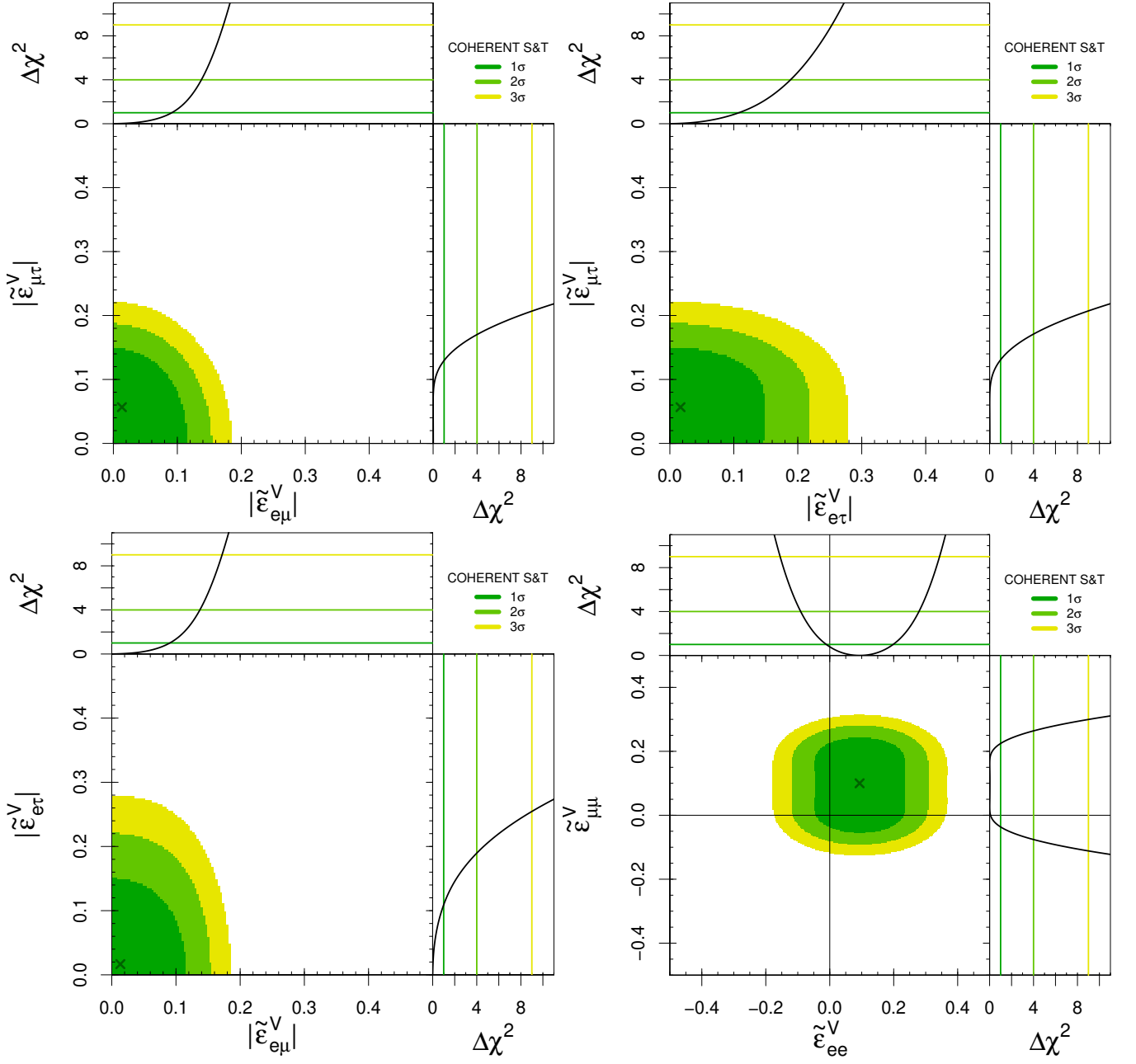


FIG. 7. General marginalized allowed regions in different planes of the optimal up-down linear combination of NSI parameters (14) and marginal $\Delta\chi^2$'s obtained from the analysis of the joint COHERENT spectral and temporal (S&T) data. The points indicate the best-fit values.

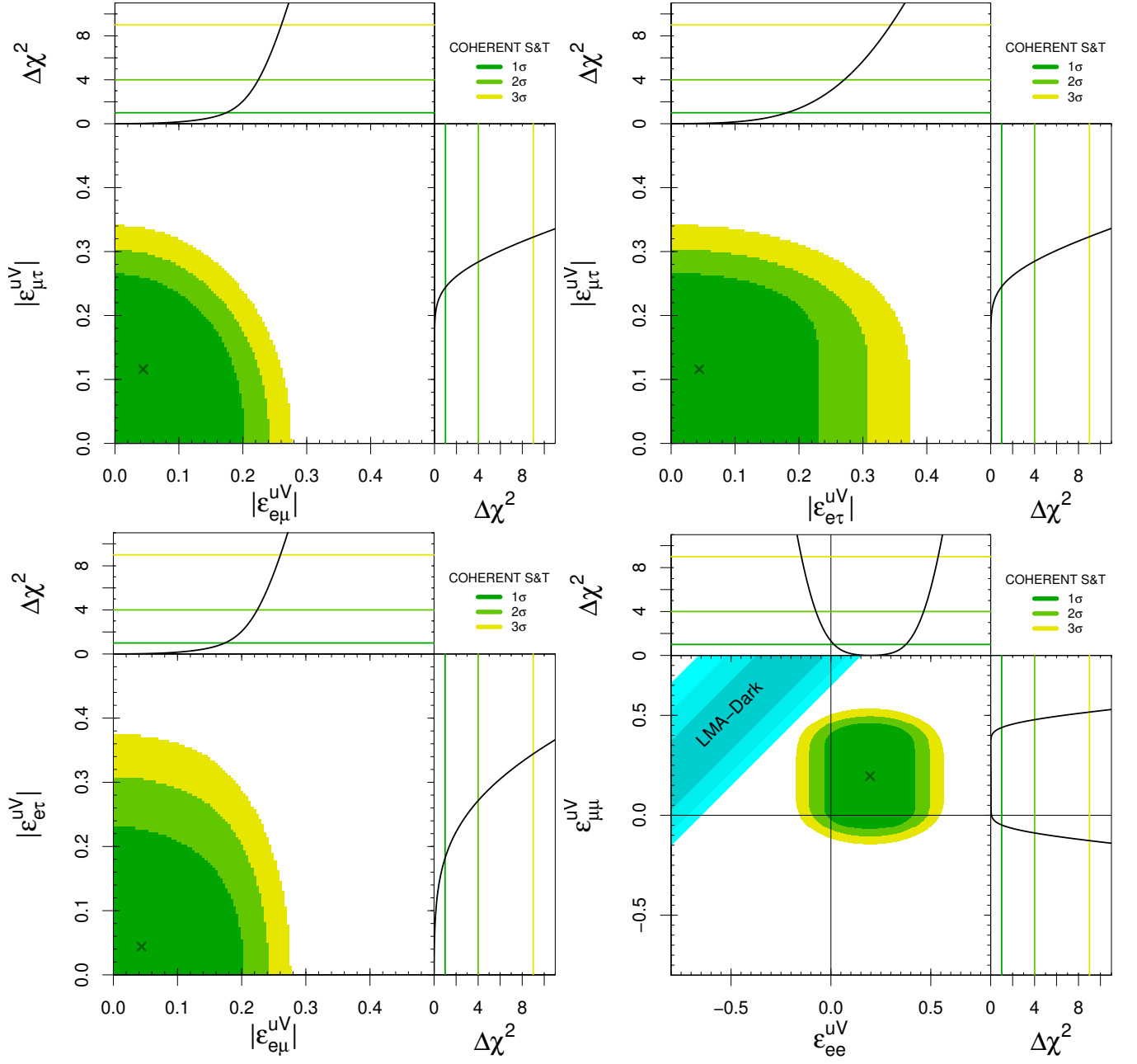


FIG. 8. Marginalized allowed regions in different planes of the NSI parameters and marginal $\Delta\chi^2$'s obtained from the analysis of the joint COHERENT spectral and temporal (S&T) data assuming interactions with up quarks only. The points indicate the best-fit values. The diagonal cyan strips in the $(\varepsilon_{ee}^{uV}, \varepsilon_{\mu\mu}^{uV})$ plane are allowed at 1σ , 2σ , and 3σ by the LMA-Dark fit of solar neutrino data [11].

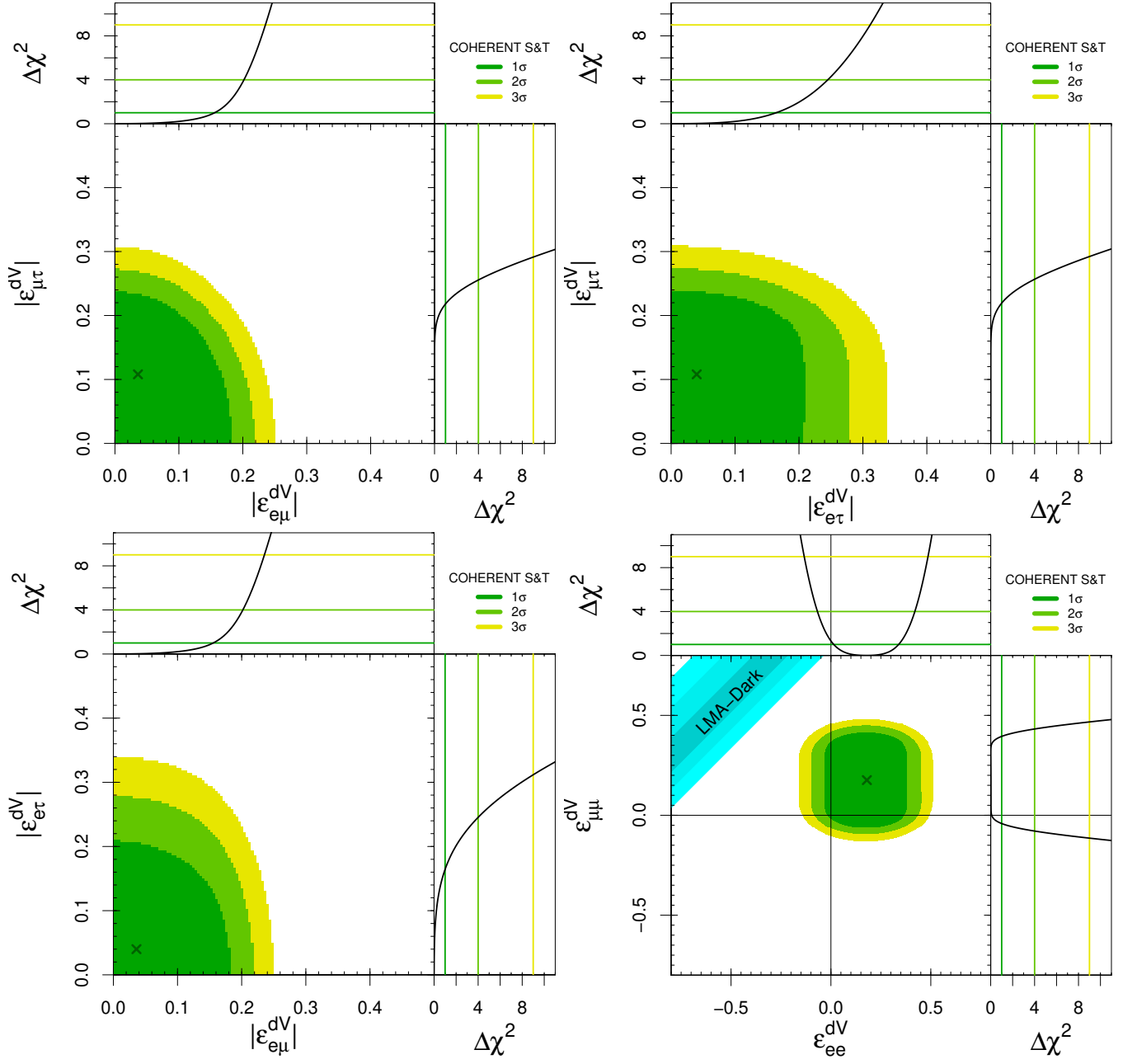


FIG. 9. Marginalized allowed regions in different planes of the NSI parameters and marginal $\Delta\chi^2$'s obtained from the analysis of the joint COHERENT spectral and temporal (S&T) data assuming interactions with down quarks only. The points indicate the best-fit values. The diagonal cyan strips in the $(\epsilon_{ee}^{dV}, \epsilon_{\mu\mu}^{dV})$ plane are allowed at 1σ , 2σ , and 3σ by the LMA-Dark fit of solar neutrino data [11].

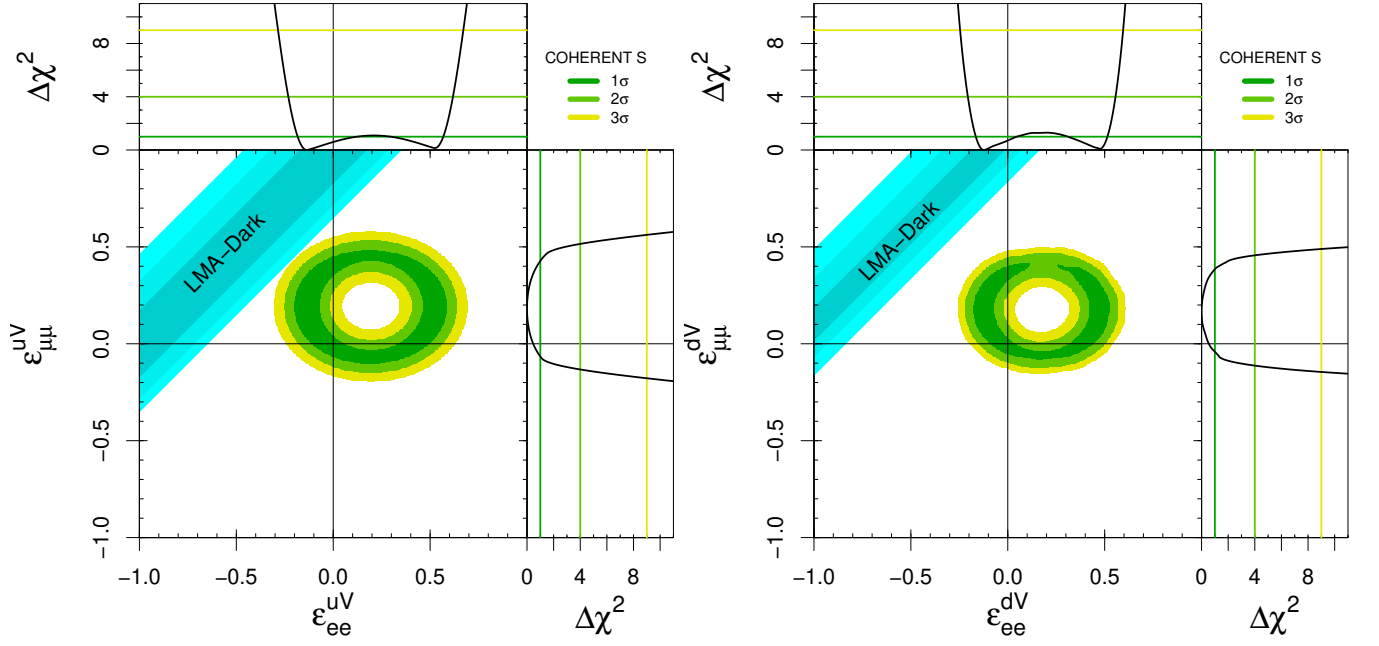


FIG. 10. Allowed regions and marginal $\Delta\chi^2$'s in the plane $(\varepsilon_{ee}^{uV}, \varepsilon_{\mu\mu}^{uV})$ assuming that only these two NSI parameters are non-vanishing (left) and in the plane $(\varepsilon_{ee}^{dV}, \varepsilon_{\mu\mu}^{dV})$ assuming that only these two NSI parameters are non-vanishing (right). Results obtained from the analysis of the COHERENT spectral (S) data alone. The diagonal cyan strips are allowed at 1σ , 2σ , and 3σ by the LMA-Dark fit of solar neutrino data [11].

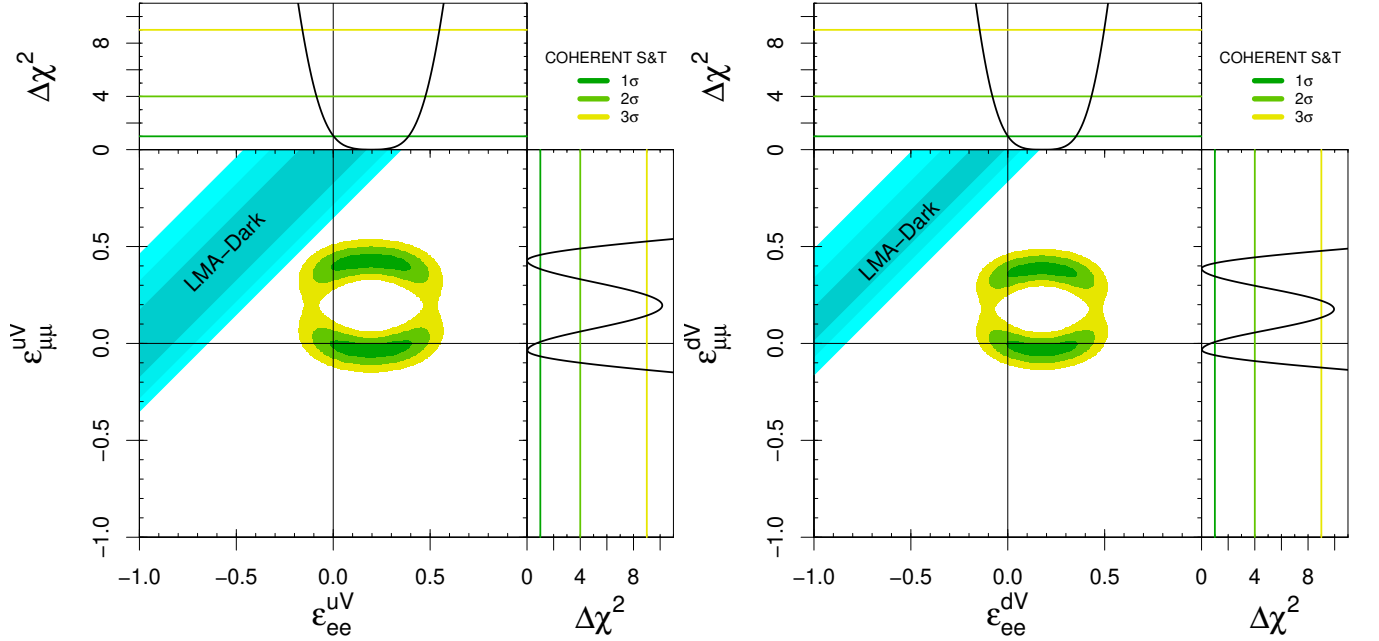


FIG. 11. Allowed regions and marginal $\Delta\chi^2$'s in the plane $(\varepsilon_{ee}^{uV}, \varepsilon_{\mu\mu}^{uV})$ assuming that only these two NSI parameters are non-vanishing (left) and in the plane $(\varepsilon_{ee}^{dV}, \varepsilon_{\mu\mu}^{dV})$ assuming that only these two NSI parameters are non-vanishing (right). Results obtained from the analysis of the joint COHERENT spectral and temporal (S&T) data. The diagonal cyan strips are allowed at 1σ , 2σ , and 3σ by the LMA-Dark fit of solar neutrino data [11].

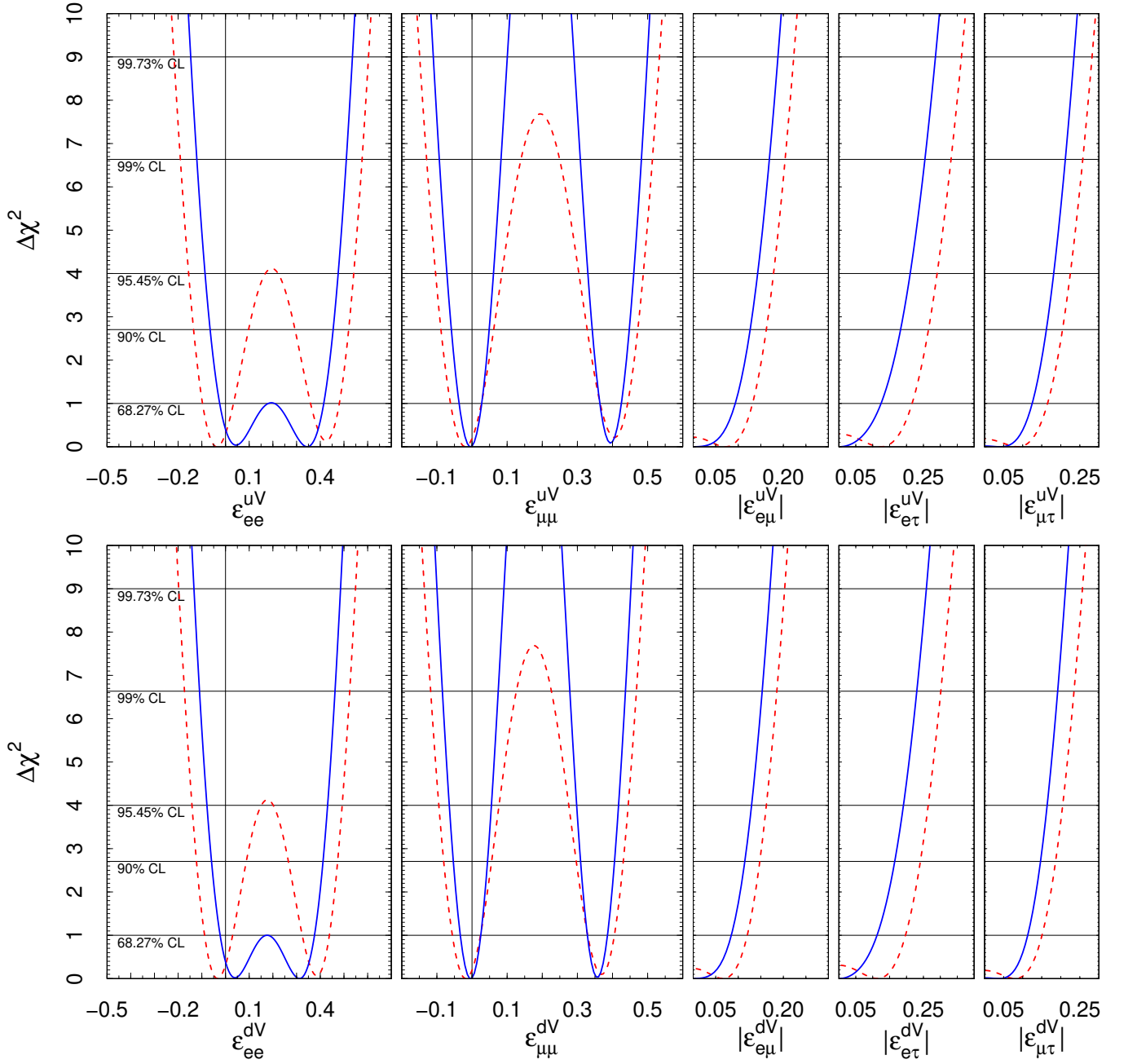


FIG. 12. $\Delta\chi^2 = \chi^2 - \chi_{\min}^2$ for each of the NSI parameters assuming it to be the only non-vanishing one. The dashed red and solid blue curves correspond, respectively, to the analysis of spectral and joint spectral and temporal COHERENT data.